
Generative Latent Flow: A Framework for Non-adversarial Image Generation

Zhisheng Xiao*

University of Chicago
zxiao@uchicago.edu

Qing Yan*

University of Chicago
yanq@uchicago.edu

Yi'an Chen

University of Chicago
yianc@uchicago.edu

Yali Amit

University of Chicago
amit@marx.uchicago.edu

Abstract

Generative Adversarial Networks (GANs) have been shown to outperform non-adversarial generative models in terms of the image generation quality by a large margin. Recently, researchers have looked into improving non-adversarial alternatives that can close the gap of generation quality while avoiding some common issues of GANs, such as unstable training and mode collapse. Examples in this direction include Two-stage VAE [12] and Generative Latent Nearest Neighbors [9]. However, a major drawback of these models is that they are slow to train, and in particular, they require two training stages. To address this, we propose Generative Latent Flow (GLF), which uses an auto-encoder to learn the mapping to and from the latent space, and an invertible flow to map the distribution in the latent space to simple i.i.d noise. The advantages of our method include a simple conceptual framework, single stage training and fast convergence. Quantitatively, the generation quality of our model significantly outperforms that of VAEs, and is competitive with GANs' benchmark on commonly used datasets.

1 Introduction

Deep generative models have recently attracted much attention in the deep learning literature. These models are used to formulate the distribution of complex data as a function of random noise passed through a network, thus making rendering samples from the distribution particularly easy. Currently, there are three major frameworks of deep generative models: Generative Adversarial Networks (GANs) [1, 13], Variational Auto-Encoders (VAEs) [2, 24] and Flow-based reversible models [3, 4, 14]. Each framework has its own advantages and disadvantages. GANs have exhibited impressive performances in a variety of tasks, including image generation [15], sequence generation [17], cross-domain transfer [16] and super-resolution [18]. Despite the success, training GANs can be challenging, since they are trained by solving a saddle point optimization problem formulated as an adversarial game between a generator that produces the samples and a discriminator which judges if the samples are real. It is well known that training GANs is unstable and extremely sensitive to hyper-parameter settings [19], and sometimes training leads to mode collapse [20], where most of the samples share some common properties. Although there have been multiple efforts to overcome the difficulties in training GANs, mainly by modifying the objective functions [22, 23, 21], researchers are also actively studying non-adversarial generative models that are known to be less affected by these issues.

*equal contribution

VAEs provide a probabilistic model for high dimensional data, and training is performed using variational inference. The log-likelihood of the data is approximated by the evidence lower bound (ELBO), which is maximized with respect to both the parameters of the generative model and the parameters of the approximation to the posterior on the latent variables conditional on the observation. VAEs have a simple probabilistic explanation and optimization objective, and the training of VAEs has proven to be more stable. With these advantages, VAEs are also widely used in many tasks such as [25, 26, 27]. Unfortunately, VAEs’ image generation quality still lies far below that of GANs, especially on large and real datasets. It is observed that VAEs tend to generate blurry images, an effect that is usually attributed to the constraint of Gaussian assumptions [12]. More details on this will be discussed later.

Flow-based models consist of a sequence of invertible transformations that are composed to define an invertible mapping between a complicated data distribution and a simple noise distribution. Since the mapping is invertible, the flows can explicitly model the data distribution and compute the exact negative log-likelihood, provided the Jacobians are easily computable. While being mathematically clear, flow-based models have one major drawback: computational complexity. It is impossible to reduce the input dimension while keeping invertibility, and thus the latent space of a flow-based model must have the same dimension as the original data space. This makes training computationally expensive. Considering the prohibitively long training time and advanced hardware requirements in training large scale flow models such as [14], we believe that it is better to apply flows to the low dimensional latent variables rather than to original data.

There are also attempts to combine various generative frameworks, mainly by trying to equip auto-encoder type models with an adversarial loss [28, 6]. While they can generate sharper samples than plain VAEs do, the instability caused by adversarial objectives is still present. Our work is motivated by [7, 9, 12], which show that non-adversarial models have the potential to generate high quality samples just as GANs do. To this end, we propose a model called Generative Latent Flow, which uses a deterministic Auto-Encoder to learn a mapping to and from a latent space, and an invertible flow that serves as both a regularizer of these mappings and an invertible transformation between the latent space distribution and a simple noise distribution.

Our contributions are summarized as follows: i) we propose Generative Latent Flow, which is a new framework of non-adversarial generative modeling. ii) compared with competing non-adversarial generative models, our model only requires one training stage and converges much faster. iii) quantitative evaluations on several commonly used image datasets show that the generation quality of our model can match the benchmarks on GANs and be competitive with state-of-the-art non-adversarial models.

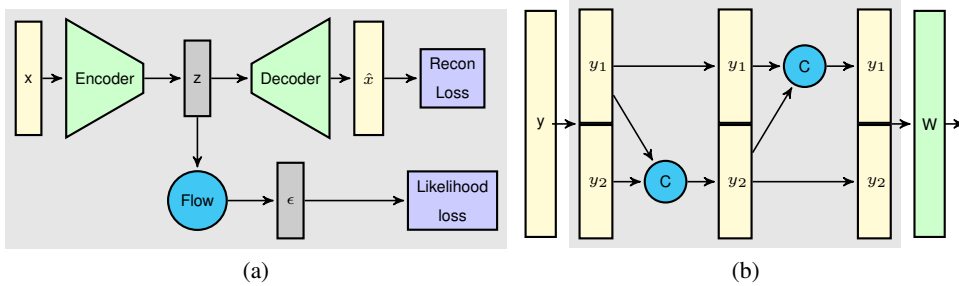


Figure 1: (a) Illustration of GLF. (b) Structure of one flow block. It splits the input into two parts $y = (y_1, y_2)$, goes through the coupling layer C , and finally applies the invertible transformation W .

2 A general framework for generative models

A general framework for generative models can be described in terms of the following three components: (1) a high dimensional data space \mathcal{X} with a complex distribution on images. (2) a latent space \mathcal{Z} , where each image $x_i \in \mathcal{X}$ is associated with a latent variable $z_i \in \mathcal{Z}$ through a decoder or generator $x_i = G(z_i)$. Note that \mathcal{Z} may or may not have lower dimensionality than \mathcal{X} , and the distribution over \mathcal{Z} can still be very complicated. (3) a noise space \mathcal{E} , in which i.i.d. noise is sampled

from a predefined distribution, such that the distribution over latent variables in \mathcal{Z} can be generated by applying a transformation F from \mathcal{E} to \mathcal{Z} . For simplicity, we can just assume the distribution on \mathcal{E} to be standard Gaussian noise.

All generative models in the deep learning literature can be described in terms of this framework. Flow-based models, GANs, and the less familiar IMLE [8] directly connect \mathcal{E} and \mathcal{X} , which makes image generation easy, as one can sample the noise in \mathcal{E} and apply the learned transformation F . However, these methods are all known to be hard to train, since finding a direct connection between highly structured data and completely unstructured noise can be very difficult. Alternatively, VAEs learn to reconstruct data through the latent space \mathcal{Z} . Reconstruction is a less demanding task than directly mapping noise to data, and therefore training a VAE is easier. However, it comes at the price of lower quality samples, as discussed in [12]. The trade-off between training and sampling can be avoided if we can design a model that connects the three spaces, with the mapping G and F together with a simple training procedure. One implementation of this idea is explored in Generative Latent Nearest Neighbors (GLANN) [9], which learns a nearest neighbor mapping between noise and the latent space. Here we present a different implementation that is more transparent and faster to train.

3 The Generative latent flow (GLF) model

Our model uses a deterministic auto-encoder composed of an encoder $E_\eta : \mathcal{X} \rightarrow \mathcal{Z}$ and decoder (generator) $G_\phi : \mathcal{Z} \rightarrow \mathcal{X}$. In addition we have a transformation F_θ from a standard Gaussian distribution to \mathcal{Z} . The transformation F_θ is defined in terms of a flow model (see below) and all three components are estimated simultaneously end to end in terms of a loss that combines the reconstruction quality and the likelihood of the encoded data z_i with respect to the transformation F_θ . The model is illustrated in Figure 1a. The details are provided in the next two sections.

3.1 Flow models for the transformation F

Flow-based generative models, which were first introduced in [3] and extended in [4, 14], are conceptually attractive due to the tractability of the explicit likelihood, and the efficient inference and sampling procedures. The core of the flow-based model is a carefully-designed invertible network that maps the training data to a simple latent distribution.

Let $z \in \mathcal{Z}$ be an observation from an unknown target distribution $z \sim p_Z$ and p_E be a simple prior distribution on latent space \mathcal{E} . Given a bijection $f_\theta : \mathcal{Z} \rightarrow \mathcal{E}$, the change of variable formula defines a model $p_\theta(z)$ with parameters θ on \mathcal{Z} by $\log p_\theta(z) = \log p_E(f_\theta(z)) + \log \left| \det \left(\frac{\partial f_\theta(z)}{\partial z} \right) \right|$, where $\frac{\partial f_\theta(z)}{\partial z}$ is the Jacobian matrix of f_θ . In order to learn the invertible transformation f_θ , the log-likelihood objective is then equivalent to

$$\min_\theta \mathcal{L}_\theta(Z) = -\frac{1}{N} \sum_{i=1}^N \log p_E(f_\theta(z_i)) - \log \left| \det \left(\frac{\partial f_\theta(z_i)}{\partial z} \right) \right| \quad (1)$$

Since the mapping is a bijection, sampling from the trained model $p_\theta(z)$ is trivial. Sample $e \sim p_E(e)$ and compute $z = f_\theta^{-1}(e)$. The key to designing a tractable flow model is defining the transformation f_θ such that the inverse transformation and the determinant of the Jacobian matrix can be efficiently computed.

We use the invertible flow to model the function $F_\theta = f_\theta^{-1}$. In our case this latent flow is easy to train due to the low-dimension of the latent variables. Note that training flow models directly in image space is hard and computationally expensive because flows have to keep the input dimension unchanged. Based on the work in [4], we adopt the following layers to form the flows used in our model.

Affine coupling layer: Given a D dimensional input data z and $d < D$, we partition the input into two vectors $z_1 = z_{1:d}$ and $z_2 = z_{d+1:D}$. The output of one affine coupling layer is given by

$$y_1 = z_1, \quad y_2 = z_2 \odot \exp(s(z_1)) + t(z_1)$$

where s and t are functions from $\mathbb{R}^d \rightarrow \mathbb{R}^{D-d}$ and \odot is the element-wise product, and the exponentiation is elementwise. The inverse of the transformation is explicit given by

$$z_1 = y_1, \quad z_2 = (y_2 - t(y_1)) \odot \exp(-s(y_1))$$

The determinant of the Jacobian matrix of this transformation is simply $\det \frac{\partial \mathbf{y}}{\partial \mathbf{z}} = \prod_{j=1}^d (\exp[s(\mathbf{z}_1)_j])$. Since computing both the inverse and the Jacobian does not require computing the inverse and Jacobian of s and t , both functions can be arbitrarily complex. See [4] for more details.

Combining coupling layers and learnable permutation: Affine coupling layers leave some components of the input data unchanged. In order to transform all the components, two affine coupling layers are combined in an alternating pattern to form a coupling block, so the unchanged components in the first layer can be transformed in the second layer. The construction of a coupling block can be viewed as a fixed permutation of dimensions of the input data. In [14], the authors also propose a generalization of the permutation operation called invertible 1×1 convolution, where the convolution weight matrix is initialized to be a rotation matrix but can be learned and updated during training. We adopt a similar idea, but since our flow is applied on a lower dimensional latent space which has only one channel, we take a more direct approach. Assume our input is an h dimensional vector y , before each coupling block, we multiply the data by an $h \times h$ weight matrix W , which is initialized to be a rotation matrix and is set to be learnable. As long as the matrix W is non-singular, the inverse of this operation can be computed, and the log-determinant of the Jacobian of the operation is straightforward: $\log \left| \det \left(\frac{d(Wy)}{dy} \right) \right| = \log |\det(W)|$. The determinant of W can be computed directly by the QR decomposition in $\mathcal{O}(h^3)$, but since the dimension of the latent space is much lower than the dimension of the original image samples, the computational cost is acceptable.

3.2 The generator G

Having defined invertible flow $F_\theta : \mathcal{E} \rightarrow \mathcal{Z}$, we still need to train a generator $G_\phi : \mathcal{Z} \rightarrow \mathcal{X}$. We use a deterministic auto-encoder composed of an encoder E_η and a decoder (generator) G_ϕ . The auto-encoder is trained to minimize the reconstruction loss, which we set to be either the common MSE loss or more advanced perceptual loss [29]. The perceptual loss is obtained by feeding both training images and reconstructed images into a pre-trained network such as VGG [30], and computing the MSE loss between some of the intermediate layer activations. It is shown that training with perceptual loss will lead to sharper outputs [31, 9]. The overall training objective is a combination of the reconstruction loss and the likelihood loss for the flow transformation:

$$\mathcal{L}(\eta, \phi, \theta) = \frac{1}{N} \sum_{i=1}^N \mathcal{L}_{\text{recon}}(\mathbf{x}_i, G_\phi(E_\eta \mathbf{x}_i)) + \beta \mathcal{L}_{\text{likelihood}}(f_\theta(E_\eta(\mathbf{x}_i)))$$

where η, ϕ are the parameters of the encoder and decoder respectively, θ is the parameter of the flow and β is a hyper-parameter that controls the relative weight of the reconstruction loss and the likelihood loss in equation (1). In summary, our proposed generative model consists of (i) a deterministic auto-encoder whose encoder E_η learns a mapping into a low dimension latent space, and whose decoder G_ϕ serves as a generator that produces samples, and (ii) a flow model F_θ that learns an invertible mapping between latent space and simple Gaussian noise. The generating process is easy: first sample a noise $e \sim \mathcal{N}(0, I)$ and then obtain a generated sample $\tilde{x} = G(F(e))$, $F = f_\theta^{-1}$. Since the highlight of our model is applying a flow on latent variables, we name it **Generative Latent Flow (GLF)**. See Figure 1a for an illustration of the GLF model.

3.3 One Stage v.s. Two Stage

Most non-adversarial generative models that claim to match the generation performance of GANs involve either two-stage training [12, 9] or distribution fitting after training [32], which can also be regarded as a two-stage procedure. In contrast, our model can work naturally in either one stage or two stages. In two-stage training, we first train an auto-encoder to form a latent space for the training images, and then train a flow model that maps the latent variables of training images to a noise distribution. In one stage training, we simply add the reconstruction loss from the auto-encoder and the likelihood loss from the flow together, and train the whole system jointly. Note that in the one-stage case, gradients of the likelihood loss will back-propagate into the encoder, so the flow not only matches the densities but also serves as a regularizer on the encoding map E encouraging the resulting latent variables to be easily transformed by the flow. This interpretation shares some similarities with VAEs: they are both auto-encoders with regularization (KL terms or likelihood loss) on the latent space. Empirically we find our model works similar or better in one-stage training, even if we manually add regularization on the latent variables in two-stage training. This suggests that the flow is indeed a good regularizer on the encoder.

4 Related Work

There are several papers focusing on the problem of mismatch between the true latent distribution and the sampling distribution in generative models. Depending on the use of random or deterministic latent variables, they can be divided into two categories.

The first type still deploy a VAE framework, with additional modifications on the sampling step. For example, “two-stage-VAE” [12] introduces another VAE on the latent space defined by the first VAE which is trained in the usual way. It claims that the mismatching problem comes from the dimensionality reduction of the first-stage VAE, and adding a second-stage VAE which preserves or even increases the dimensionality of the latent space can relieve that problem. In [33], the authors proposed to learn an extra rule that tells whether to accept or reject samples from $p(z)$. It does not solve the mismatch problem but learns a link between the marginal $q_\theta(z)$ induced by the approximate posterior and $p(z)$.

The second type of method uses a deterministic mapping from data to latent variable, either through an encoder or by optimizing explicitly over the latent variable space, and then fits the latent variables computed from the data with a sampling scheme. GLANN [9] learns a deterministic latent representation by GLO [7] and uses IMLE [8] to match the densities of latent space and noise space. However, training GLO is very slow, thus GLANN needs many epochs to converge. [32] trains a regularized Auto-Encoder and then fits a mixture Gaussian distribution over the latent space. Our method belongs to this type, but by employing the flow transformation, our model can more easily match the densities. Moreover, it is possible to train our method end-to-end in one stage.

WAE [34] can be thought of as either a type 1 or type 2 method, depending on the setting of $q_\theta(z|x)$ (when $q_\theta(z|x)$ is a delta distribution, it uses a deterministic auto-encoder). It also incorporates the idea of combining auto-encoder with density matching but with a different loss: it uses Wasserstein distance to measure the goodness of AE (or VAE) and either GAN-based or MMD-based [35] loss to measure the distance between z and ε (or $q_\theta(z)$ and $p(z)$).

Note that there is also work combining VAE and flows [36, 37, 38]. Although similar in name, our model is completely different. This work use normalizing flows to connect the encoder and decoder, aiming to complicate the posterior distribution of z . Instead of forcing more complicated posterior distributions which may lead to better results in the likelihood but not helpful for generation quality [12], our flow is designed to improve the quality of generation by matching the density of the latent variables and noise.

5 Experiments

To evaluate the performance of our method, we perform both quantitative and qualitative evaluations on four commonly used datasets for generative models: MNIST [39], Fashion MNIST [40], CIFAR-10 [41] and CelebA [10]. MNIST and Fashion-MNIST contain 50k 28×28 grey-scale images, and CIFAR-10 contains 50k 32×32 color images. We use the original images in the training sets for these three datasets. CelebA contains 220k images of human faces, and we follow the same pre-processing as in [42]: center crop to 160×160 and then resize to 64×64 . Throughout the experiments, we use 20-dimensional latent variables for MNIST and Fashion MNIST, and 64-dimensional latent variables for CIFAR-10 and CelebA.

5.1 Models and Settings

[42] adopted a common network architecture based on InfoGAN [43] for all the GANs they tested. In order to make fair comparisons without designing arbitrarily large networks to achieve better performance, we use the same generator architecture of InfoGAN as our decoder, and we make the encoder to be symmetric to the decoder. For the flow applied on latent variables, we use 4 blocks defined as in Figure 1b, where each block contains 4 fully connected layers each with k hidden units. For MNIST and Fashion MNIST, $k = 32$, while for CIFAR-10 and CelebA, $k = 100$. Note that the flow only adds a negligible parameter overhead on the auto-encoder (less than 3%). In particular, our Flow has 95% less parameters than the second-stage VAE in [12], which uses 3 fully connected layers each with 1024 hidden units. For details on network structures, see Appendix A.

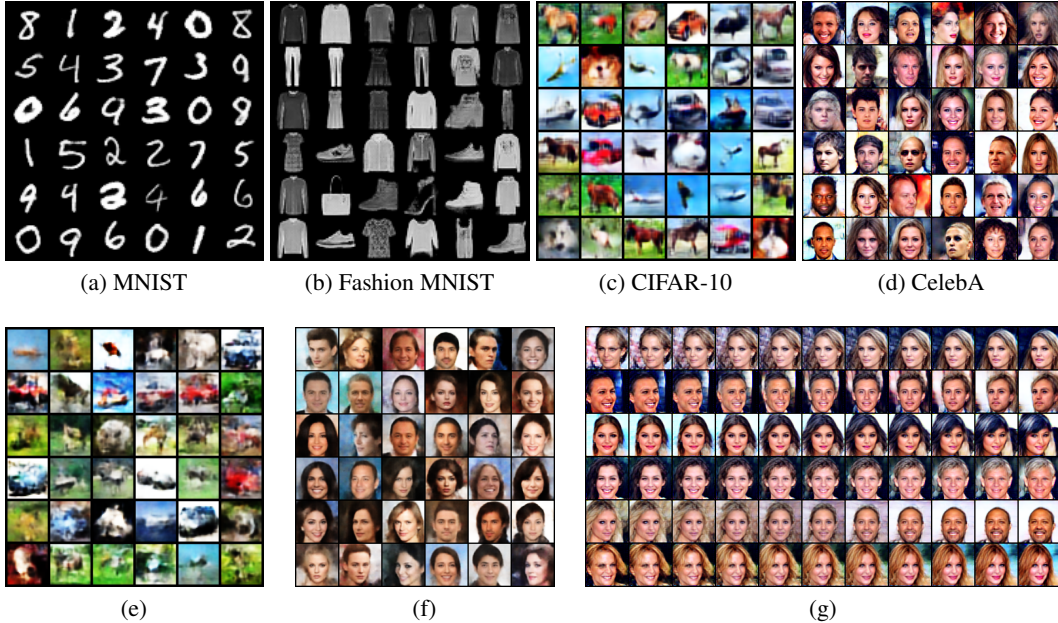


Figure 2: (a)-(d): Randomly generated samples from our method trained in one-stage with perceptual loss. (e) and (f): Randomly generated samples from our method trained in one-stage with MSE loss on CIFAR-10 and CelebA. (g): Random noise interpolation on CelebA using models trained in one-stage with perceptual loss.

Although we could possibly obtain better results by fine tuning the hyper-parameter β that controls the relative weight of the two terms in objective function, for simplicity, we fix $\beta = 1$ throughout our experiments. We use both VGG perceptual loss and MSE loss as the reconstruction loss to train our model, and the experimental settings corresponding to the two losses are slightly different. Due to space limitation, we present the detailed settings of our experiments in Appendix B.

5.2 Metrics

The evaluation of generative models is a nontrivial question [44]. One popular metric is the Fréchet Inception Distance (FID) [45]. FID is computed by first extracting features of a set of real images x and a set of generated images g from an intermediate layer of the Inception network. Each set of features is fitted with a Gaussian distribution, yielding means μ_x, μ_g and co-variances matrices Σ_x, Σ_g . The FID score is defined to be the Fréchet distance between these two Gaussians:

$$\text{FID}(x, g) = \|\mu_x - \mu_g\|_2^2 + \text{Tr} \left(\Sigma_x + \Sigma_g - 2(\Sigma_x \Sigma_g)^{\frac{1}{2}} \right)$$

It is claimed that the FID score is sensitive to mode collapse and correlates well with human perception of generator quality. We use FID score as our main evaluation metric for generation quality. Very recently, [46] propose to use Precision and Recall for Distributions (PRD) which can assess both the quality and diversity of generated samples. We also include PRD in our studies. See Appendix C.

5.3 Results

Table 1 summarizes our main results on FID score. The results on GANs are adopted from [42], where the authors conduct standardized and comprehensive evaluations of 7 representative adversarial models (DCGAN, LSGAN, NSGAN, W-GAN, WGAN GP, DRAGAN, BEGAN) as well as VAE. In [42], results are obtained from large-scale hyper-parameter searches for each dataset, and therefore, although they do not claim their scores to be the state-of-the-art performances of given models, their results can serve as a strong baseline. The results on GLANN and Two-stage VAE are adopted from [9] and [12], respectively. Their settings, such as network structures, largely follow that of [42], so we can directly compare them with our results. In order to compare our method with VAEs in exactly

Table 1: FID score comparisons across different models. For our reported results, we executed 10 independent trials and report the mean and standard deviation of the FID scores. Each trail is computing the FID between 10k generated images and 10k real images.

	MNIST	Fashion	CIFAR-10	CelebA
MM GAN	9.8 ± 0.9	29.6 ± 1.6	72.7 ± 3.6	65.6 ± 4.2
NS GAN	6.8 ± 0.5	26.5 ± 1.6	58.5 ± 1.9	55.0 ± 3.3
LSGAN	7.8 ± 0.6	30.7 ± 2.2	87.1 ± 47.5	53.9 ± 2.8
WGAN	6.7 ± 0.4	21.5 ± 1.6	55.2 ± 2.3	41.3 ± 2.0
WGAN GP	20.3 ± 5.0	24.5 ± 2.1	55.8 ± 0.9	30.3 ± 1.0
DRAGAN	7.6 ± 0.4	27.7 ± 1.2	69.8 ± 2.0	42.3 ± 3.0
BEGAN	13.1 ± 1.0	22.9 ± 0.9	71.4 ± 1.6	38.9 ± 0.9
VAE	24.4 ± 0.3	45.7 ± 0.4	124.0 ± 0.6	70.6 ± 0.5
Two-Stage VAE	12.6 ± 1.5	29.3 ± 1.0	72.9 ± 0.9	44.4 ± 0.7
GLANN	8.6 ± 0.1	13.0 ± 0.1	46.5 ± 0.2	46.3 ± 0.1
GLF (ours)	7.9 ± 0.1	15.1 ± 0.2	59.8 ± 0.4	44.1 ± 0.2

the same settings, we trained our own VAEs and report the results instead of directly copying them from [42].

GLANN is trained with the perceptual loss, while Two-stage VAE and our VAE use MSE loss. The results of our method (GLF) presented in Table 1 are obtained from one-stage training with perceptual loss. Comparisons of perceptual v.s. MSE loss as well as one-stage v.s. two-stage training on our method are in Table 2. One particular detail worth noting is that, in Two-stage VAE, the authors applied 128×128 center-crop before re-sizing on CelebA, while we follow the settings in [42] where 160×160 center-crop is used. With smaller center-crops the human faces occupy a larger portion of the image with less background, making the generative modeling easier. Therefore, we expect their results to be worse when using our pre-processing on CelebA.

From Table 1, we observe that in general, our method has generation quality that outperforms VAEs by a large margin, and is competitive with a variety of GANs. Moreover, our method achieves the lowest FID among competing non-adversarial models on two datasets. Note that while achieving comparable or better performances, our method needs significantly fewer training epochs than GLANN and Two-stage VAE (See 5.3.1 and Appendix B). Our results strongly support the claim that GLF is a powerful non-adversarial generative model which can generate high quality samples while converging faster than competing models.

Qualitative results are shown in Figure 2. The samples of MNIST and Fashion MNIST look visually similar across different loss functions, so we only present perceptual loss samples. Clearly our model can generate sharp and diverse samples on each dataset, especially when trained with perceptual loss. In Figure 2g, we show images generated by interpolating between two random noise samples. For more qualitative results, see Appendix D.

5.3.1 Comparisons

Choice of loss function: The choice of reconstruction loss can have significant impact on generation. [9] suggests that using perceptual loss leads to higher generation quality. We confirmed this by comparing our models trained with perceptual loss and MSE loss in Table 2. Note that the results from training GLF with MSE loss are comparable with that of Two-stage VAE in Table 1, which is also trained with MSE loss. This suggest that our method is competitive with current state-of-the-art non-adversarial generative models, independent of the choice of reconstruction loss function.

One-stage v.s two-stage training: As discussed above, one of the main advantage of our method over other non-adversarial models is that it can be trained end-to-end in one stage. In Table 2 we report the performance of two-stage training. We observe that the results of two-stage training are slightly better than one-stage. The comparable results suggest that one-stage training can achieve good generation quality and thus two-stage training may not be necessary. The results further imply that the flow is a good regularizer on the latent space.

Table 2: FID score comparisons between different reconstruction loss functions, top: one-stage, bottom: two-stage.

	MNIST	Fashion	CIFAR-10	CelebA
MSE one-stage	12.9 ± 0.2	27.1 ± 0.3	76.5 ± 0.6	51.4 ± 0.5
Perceptual one-stage	7.9 ± 0.1	15.1 ± 0.2	59.8 ± 0.4	44.1 ± 0.2
MSE two-stage	11.0 ± 0.1	26.3 ± 0.4	83.8 ± 0.4	54.6 ± 0.2
Perceptual two-stage	6.9 ± 0.1	13.7 ± 0.1	59.3 ± 0.2	43.2 ± 0.3

Comparison with ex-post density fitting: Recently, [32] proposed to train a regularized auto-encoder and then fit either a Gaussian or Gaussian mixture distribution on the latent space. It is a conceptually simple generative model, and they report impressive FID scores. However, their experimental settings are different from ours (they use deeper networks and different image pre-processing method), so we do not directly report their results. Instead, we take their approach to fit a density on the latent space of the auto-encoder models we have trained with perceptual loss, and compare them with GLF. Results are presented in Table 3, where \mathcal{N} means fitting a full co-variance Gaussian and GMM means fitting a 10-component Gaussian mixture. Our methods outperforms ex-post density fitting on the latent space of an auto-encoder, especially on CIFAR-10 and CelebA dataset where the latent dimensions are larger. This suggests that the flow in our model does a good job matching the density in the latent space.

Table 3: FID score comparisons between our models and ex-post density fitting.

	MNIST	Fashion	CIFAR-10	CelebA
\mathcal{N}	30.1 ± 0.3	54.0 ± 0.6	71.5 ± 0.8	59.1 ± 0.5
GMM	8.1 ± 0.1	17.3 ± 0.5	63.8 ± 0.6	49.1 ± 0.3
GLF	7.9 ± 0.1	15.1 ± 0.2	59.8 ± 0.4	44.1 ± 0.2

Training time: In comparison to the two stage methods GLANN and Two-stage VAE, GLF requires much less training epochs to generate high quality samples. In Table 4 we compare the number of epochs for the three methods. Note that an epoch in GLANN is slower than the other two methods because of the need to optimize over the latent variable. Here we present the number of training epochs for our model with perceptual loss (for number of epochs with MSE loss, see Appendix B1).

Table 4: Comparison of training epochs for Two-stage VAE, GLANN, GLF

	MNIST	Fashion	CIFAR-10	CelebA
TwoVAE First/Second	400/800	400/800	1000/2000	120/300
GLANN	500/50	500/50	500/50	500/50
GLF First/Second	80/80	80/80	200/100	40/40

6 Conclusion

In this paper we introduced a novel non-adversarial generative model which uses an auto-encoder to learn a mapping from the images a latent space and an invertible flow to match the density of the latent variables with noise. Our model achieves good results in image generation, outperforming several recently proposed non-adversarial models. Compared to other non-adversarial models, our method needs much fewer iterations, and more importantly, can be trained end-to-end in one-stage with comparable performance to tow-stage training. This opens the door to learning the latent density in an end-to-end fashion. Our model has many possible extensions, including conditional generation and learning semantically disentangled representations. These are left for future work.

References

- [1] Goodfellow, Ian, et al. "Generative adversarial nets." In *Advances in Neural Information Processing Systems*, 2014.
- [2] Kingma, Diederik P., and Max Welling. "Auto-encoding variational bayes." *arXiv preprint arXiv:1312.6114*, 2013.
- [3] Dinh, Laurent, David Krueger, and Yoshua Bengio. "Nice: Non-linear independent components estimation." *arXiv preprint arXiv:1410.8516*, 2014.
- [4] Dinh, Laurent, Jascha Sohl-Dickstein, and Samy Bengio. "Density estimation using real nvp." *arXiv preprint arXiv:1605.08803*, 2016.
- [5] Hu, Zhiting, et al. "On unifying deep generative models." *arXiv preprint arXiv:1706.00550*, 2017.
- [6] Mescheder, Lars, Sebastian Nowozin, and Andreas Geiger. "Adversarial variational bayes: Unifying variational autoencoders and generative adversarial networks." In *Proceedings of the 34th International Conference on Machine Learning-Volume 70*, JMLR. org, 2017.
- [7] Bojanowski, Piotr, Armand Joulin, David Lopez-Paz, and Arthur Szlam. "Optimizing the latent space of generative networks." *arXiv preprint arXiv:1707.05776*, 2017.
- [8] Li, Ke, and Jitendra Malik. "Implicit maximum likelihood estimation." *arXiv preprint arXiv:1809.09087*, 2018.
- [9] Hoshen, Yedid, and Jitendra Malik. "Non-Adversarial Image Synthesis with Generative Latent Nearest Neighbors." *arXiv preprint arXiv:1812.08985*, 2018.
- [10] Liu, Ziwei, et al. "Deep learning face attributes in the wild." In *Proceedings of the IEEE international conference on computer vision*, 2015.
- [11] Heusel, Martin, et al. "Gans trained by a two time-scale update rule converge to a nash equilibrium." *arXiv preprint arXiv:1706.08500 12.1*, 2017.
- [12] Dai, Bin, and David Wipf. "Diagnosing and enhancing vae models." *arXiv preprint arXiv:1903.05789*, 2019.
- [13] Radford, Alec, Luke Metz, and Soumith Chintala. "Unsupervised representation learning with deep convolutional generative adversarial networks." *arXiv preprint arXiv:1511.06434*, 2015.
- [14] Kingma, Durk P., and Prafulla Dhariwal. "Glow: Generative flow with invertible 1x1 convolutions." In *Advances in Neural Information Processing Systems*, 2018.
- [15] Brock, Andrew, Jeff Donahue, and Karen Simonyan. "Large scale gan training for high fidelity natural image synthesis." *arXiv preprint arXiv:1809.11096*, 2018.
- [16] Zhu, Jun-Yan, et al. "Unpaired image-to-image translation using cycle-consistent adversarial networks." In *Proceedings of the IEEE international conference on computer vision*, 2017.
- [17] Yu, Lantao, et al. "Seqgan: Sequence generative adversarial nets with policy gradient." In *Thirty-First AAAI Conference on Artificial Intelligence*, 2017.
- [18] Ledig, Christian, et al. "Photo-realistic single image super-resolution using a generative adversarial network." In *Proceedings of the IEEE conference on computer vision and pattern recognition*, 2017.
- [19] Salimans, Tim, et al. "Improved techniques for training gans." In *Advances in neural information processing systems*, 2016.
- [20] Goodfellow, Ian. "NIPS 2016 tutorial: Generative adversarial networks." *arXiv preprint arXiv:1701.00160*, 2016.
- [21] Srivastava, Akash, et al. "Veegan: Reducing mode collapse in gans using implicit variational learning." In *Advances in Neural Information Processing Systems*, 2017.

- [22] Arjovsky, Martin, Soumith Chintala, and Léon Bottou. "Wasserstein gan." *arXiv preprint arXiv:1701.07875*, 2017.
- [23] Metz, Luke, et al. "Unrolled generative adversarial networks." *arXiv preprint arXiv:1611.02163*, 2016.
- [24] Rezende, Danilo Jimenez, Shakir Mohamed, and Daan Wierstra. "Stochastic backpropagation and approximate inference in deep generative models." *arXiv preprint arXiv:1401.4082*, 2014.
- [25] Yan, Xinchun, et al. "Attribute2image: Conditional image generation from visual attributes." In *European Conference on Computer Vision*, Springer, Cham, 2016.
- [26] Shen, Tianxiao, et al. "Style transfer from non-parallel text by cross-alignment." In *Advances in neural information processing systems*, 2017.
- [27] Miao, Yishu, Lei Yu, and Phil Blunsom. "Neural variational inference for text processing." In *International conference on machine learning*, 2016.
- [28] Makhzani, Alireza, et al. "Adversarial autoencoders." *arXiv preprint arXiv:1511.05644*, 2015.
- [29] Johnson, Justin, Alexandre Alahi, and Li Fei-Fei. "Perceptual losses for real-time style transfer and super-resolution." In *European conference on computer vision*, Springer, Cham, 2016.
- [30] Simonyan, Karen, and Andrew Zisserman. "Very deep convolutional networks for large-scale image recognition." *arXiv preprint arXiv:1409.1556*, 2014.
- [31] Hou, Xianxu, et al. "Deep feature consistent variational autoencoder." In *2017 IEEE Winter Conference on Applications of Computer Vision (WACV)*, IEEE, 2017.
- [32] Partha Ghosh and Mehdi S. M. Sajjadi and Antonio Vergari and Michael J. Black and Bernhard Scholkopf. "From Variational to Deterministic Autoencoders", *arxiv preprint arxiv 1903.12436*, 2019
- [33] Bauer, Matthias, and Andriy Mnih. "Resampled Priors for Variational Autoencoders." *arXiv preprint arXiv:1810.11428*, 2018
- [34] Tolstikhin, Ilya, Olivier Bousquet, Sylvain Gelly, and Bernhard Schoelkopf. "Wasserstein auto-encoders." *arXiv preprint arXiv:1711.01558*, 2017.
- [35] Gretton, Arthur, et al. "A kernel two-sample test." In *Journal of Machine Learning Research*, 2012.
- [36] Kingma, Durk P., et al. "Improved variational inference with inverse autoregressive flow." In *Advances in neural information processing systems*, 2016.
- [37] Rezende, Danilo Jimenez, and Shakir Mohamed. "Variational inference with normalizing flows." *arXiv preprint arXiv:1505.05770*, 2015.
- [38] Berg, Rianne van den, et al. "Sylvester normalizing flows for variational inference." *arXiv preprint arXiv:1803.05649*, 2018.
- [39] Y. LeCun and C. Cortes. MNIST handwritten digit database. 2010.
- [40] Xiao, Han, Kashif Rasul, and Roland Vollgraf. "Fashion-mnist: a novel image dataset for benchmarking machine learning algorithms." *arXiv preprint arXiv:1708.07747*, 2017.
- [41] A. Krizhevsky. Learning multiple layers of features from tiny images. Technical report, Citeseer, 2009
- [42] Lucic, Mario, et al. "Are GANs created equal." A Large-Scale Study. *arXiv preprint arXiv:1711.10337*, 2017.
- [43] Chen, Xi, et al. "Infogan: Interpretable representation learning by information maximizing generative adversarial nets." In *Advances in neural information processing systems*, 2016.

- [44] Theis, Lucas, Aäron van den Oord, and Matthias Bethge. "A note on the evaluation of generative models." *arXiv preprint arXiv:1511.01844*, 2015.
- [45] Heusel, Martin, et al. "Gans trained by a two time-scale update rule converge to a nash equilibrium." *arXiv preprint arXiv:1706.08500*, 2017.
- [46] Sajjadi, Mehdi SM, et al. "Assessing generative models via precision and recall." In *Advances in Neural Information Processing Systems*, 2018.
- [47] Kingma, Diederik P., and Jimmy Ba. "Adam: A method for stochastic optimization." *arXiv preprint arXiv:1412.6980*, 2014.
- [48] Reddi, Sashank J., Satyen Kale, and Sanjiv Kumar. "On the convergence of adam and beyond." *arXiv preprint arXiv:1904.09237*, 2019.

Table 5: Network structure for auto-encoder

Encoder	Decoder
Input x	Input z
4×4 Conv ₆₄ , ReLU	FC $n_z \rightarrow 1024$, BN, ReLU
4×4 Conv ₁₂₈ , BN, ReLU	FC $1024 \rightarrow 128 \times M \times M$, BN, ReLU
Flatten, FC $128 \times M \times M \rightarrow 1024$, BN, ReLU	4×4 Deconv ₆₄ , BN, ReLU
FC $1024 \rightarrow n_z$	4×4 Deconv ₁₂₈ , Tanh

Appendices

A Network Architectures

In this section we provide Table 5 that summarizes the auto-encoder network structure. The network structure is adopted from InfoGAN[43], and the difference between the networks we used for each dataset is the size of the fully connected layers, which depends on the size of the image. All convolution and deconvolution layers have stride = 2 and padding = 1 to ensure the spatial dimension decreases/increases by a factor of 2. M is simply the size of an input image divided by 4. Specifically, for MNIST and Fashion MNIST, $M = 7$; for CIFAR-10, $M = 8$; for CelebA, $M = 16$. BN stands for batch normalization.

B Experiment Settings

In this section, we present the details of our experimental settings. The major differences in the settings come from the choice of reconstruction loss for the auto-encoder, so we introduce the settings corresponds to different reconstruction loss separately. Since the settings for MNIST and Fashion MNIST are exactly the same, for simplicity we only mention MNIST. In general, we found that training with MSE loss requires a larger number of epochs. We did not conduct a wide range hyper-parameter search, and the choice of settings was not guided by performance. For example, we use smaller batch sizes when training with perceptual loss simply because it requires more memory (the VGG network has to be loaded into the GPU).

B.1 Settings for using MSE loss

For one stage training, models are trained for 100 epochs on MNIST, 300 epochs on CIFAR-10 and 120 epochs on CelebA. For two-stage training, Both AEs and flows are trained for the above number of epochs, except for CIFAR-10 where only 100 epochs for the flow is enough. Batch sizes are set to 256 for MNIST and CIFAR-10, and 128 for CelebA. We use the Adam[47] optimizer for flows and AEs, and we use AMSgrad[48] for the flow’s Adam optimizer. The initial learning rate is 10^{-3} for all models, and the learning rate is halved every 40 epochs for MNIST and CelebA and every 50 epochs for CIFAR-10. For two-stage training, the AEs are trained with the same learning rate schedule while the flows are trained with constant learning rate 10^{-3} .

B.2 Settings for perceptual loss

For one stage training, models are trained for 80 epochs on MNIST, 200 epochs on CIFAR-10 and 40 epochs on CelebA. For two-stage training, Both AEs and flows are trained with these numbers of epochs, except for CIFAR-10 where only 100 epochs for the flow is enough. Batch sizes are set to be 128 for MNIST and CIFAR-10, and 64 for CelebA. We use Adam[47] optimizer for both flows and AEs, and we use AMSgrad[48] for the flow Adam optimizer. The initial learning rate is 10^{-3} for all models, and the learning rate is halved every 40 epochs for MNIST and every 50 epochs for CIFAR-10. The learning rate is fixed for CelebA. For two-stage training, the AEs are trained with the same learning rate schedule while the flows are trained with constant learning rate 10^{-3} .

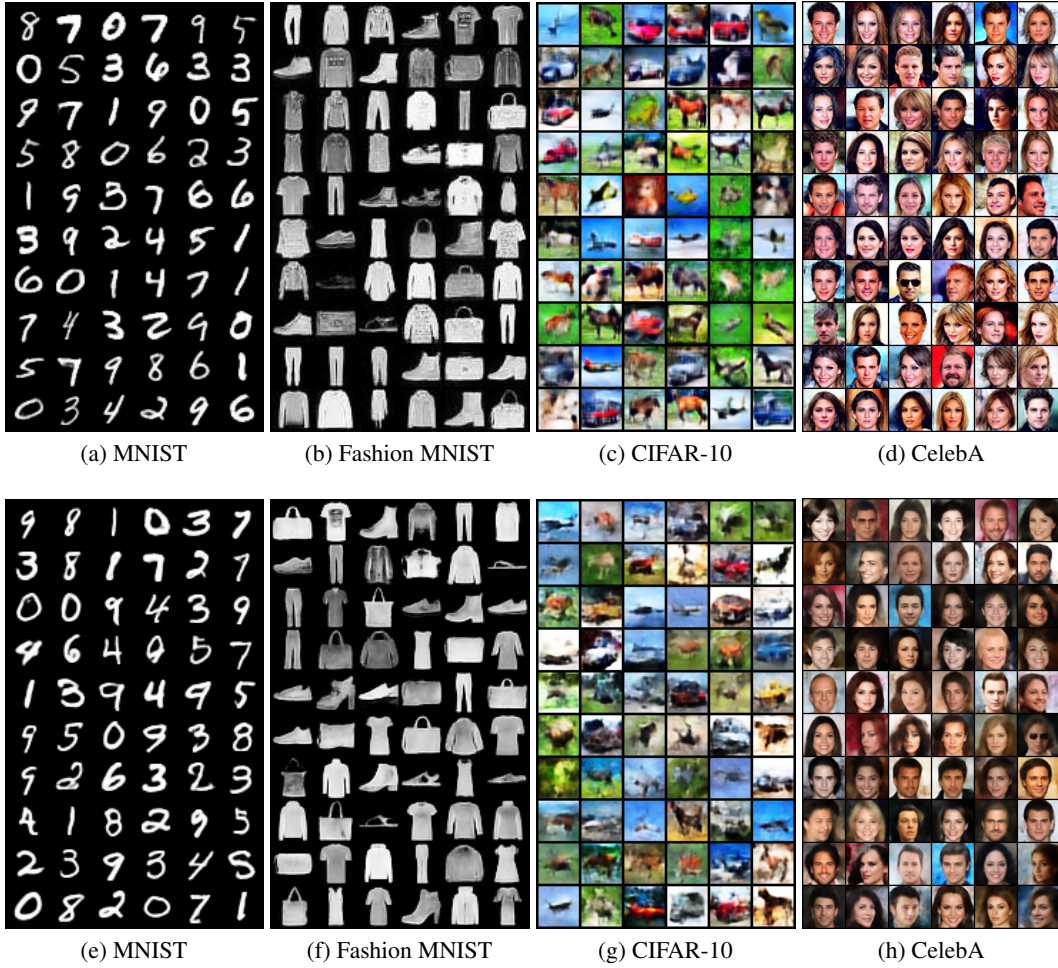


Figure 3: (a)-(d) Randomly generated samples from our method trained in one stage with perceptual loss. (e)-(h) Randomly generated samples from our method trained in one stage with MSE loss.

C Precision and Recall

In this section, we report the precision and recall (PRD) evaluation of our randomly generated samples on each dataset in Table 6. The two numbers in each entry are $F_8, F_{\frac{1}{8}}$ that captures recall and precision. See [46] for more details. We report the PRD for our models trained with perceptual loss.

Table 6: Evaluation of random sample quality by precision / recall. Higher numbers are better.

	MNIST	Fashion	CIFAR-10	CelebA
One-stage	(0.981, 0.963)	(0.974, 0.955)	(0.685, 0.805)	(0.447, 0.726)
Two-stage	(0.983, 0.972)	(0.983, 0.950)	(0.510, 0.613)	(0.437, 0.717)

D More qualitative results

In Figure 3 4, we show more samples of each dataset generated by one stage GLF and two stage GLF. In Figure 5, we show more examples of interpolations between two randomly sampled noises on CelebA dataset.

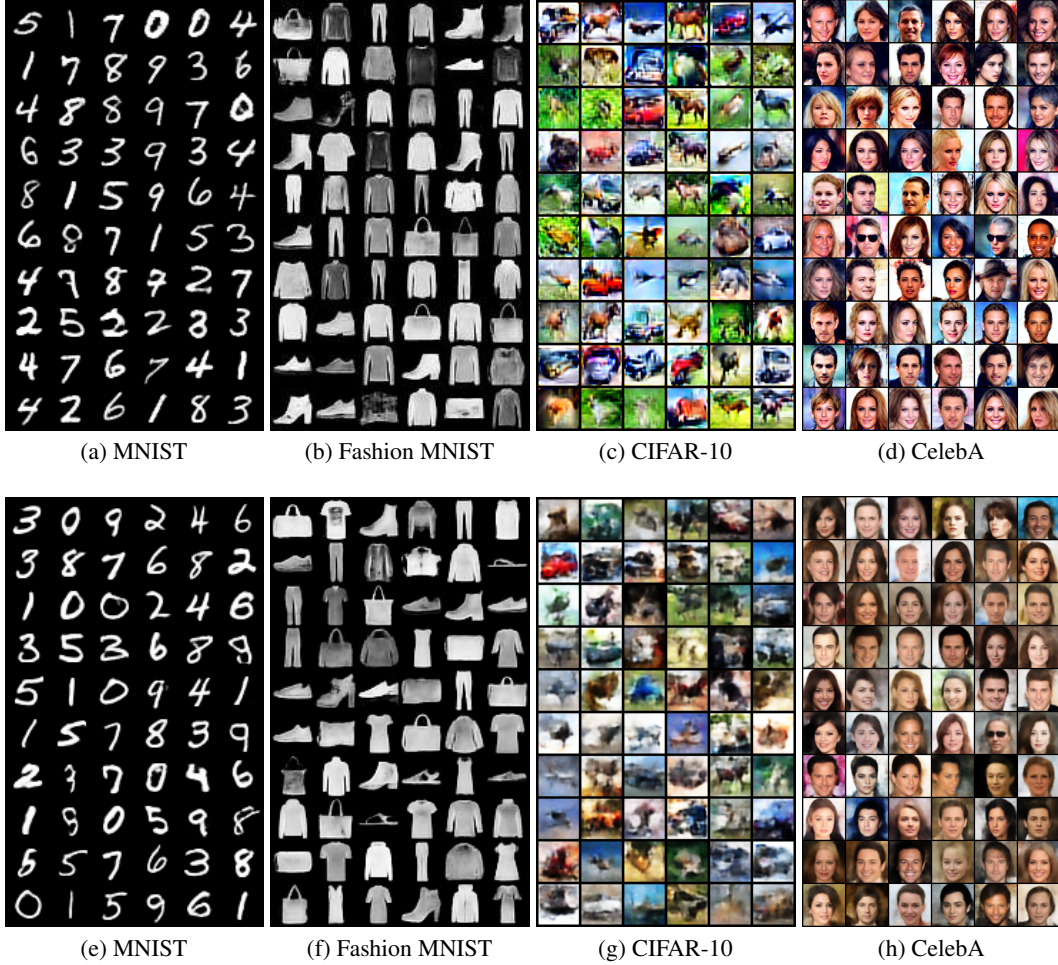


Figure 4: (a)-(d) Randomly generated samples from our method trained in two stages with perceptual loss. (e)-(h) Randomly generated samples from our method trained in two stages with MSE loss.



Figure 5: Noise interpolation on CelebA